

# Two-dimensional quantum droplets in binary quadrupolar condensates

Aowei Yang<sup>1</sup>, Jiahao Zhou<sup>1</sup>, Xiaoqing Liang<sup>1</sup>, Guilong Li<sup>1</sup>, Bin Liu<sup>1,2,\*</sup>, Huan-Bo Luo<sup>1,2,3,†</sup>, Boris A Malomed<sup>4,5</sup>, and Yongyao Li<sup>1,2</sup>

<sup>1</sup>*School of Physics and Optoelectronic Engineering, Foshan University, Foshan 528000, China*

<sup>2</sup>*Guangdong-Hong Kong-Macao Joint Laboratory for Intelligent Micro-Nano Optoelectronic Technology, Foshan University, Foshan 528000, China*

<sup>3</sup>*Department of Physics, South China University of Technology, Guangzhou 510640, China*

<sup>4</sup>*Department of Physical Electronics, School of Electrical Engineering, Faculty of Engineering, and Center for Light-Matter Interaction, Tel Aviv University, Tel Aviv 69978, Israel and*

<sup>5</sup>*Instituto de Alta Investigación, Universidad de Tarapacá, Casilla 7D, Arica, Chile*

We study the stability and characteristics of two-dimensional (2D) quasi-isotropic quantum droplets (QDs) of fundamental and vortex types, formed by binary Bose-Einstein condensate with magnetic quadrupole-quadrupole interactions (MQQIs). The magnetic quadrupoles are built as pairs of dipoles and antidipoles polarized along the  $x$ -axis. The MQQIs are induced by applying an external magnetic field that varies along the  $x$ -axis. The system is modeled by the Gross-Pitaevskii equations including the MQQIs and Lee-Huang-Yang correction to the mean-field approximation. Stable 2D fundamental QDs and quasi-isotropic vortex QDs with topological charges  $S \leq 4$  are produced by means of the imaginary-time-integration method for configurations with the quadrupoles polarized parallel to the system's two-dimensional plane. Effects of the norm and MQQI strength on the QDs are studied in detail. Some results, including an accurate prediction of the effective area, chemical potential, and peak density of QDs, are obtained in an analytical form by means of the Thomas-Fermi approximation. Collisions between moving QDs are studied by means of systematic simulations.

## I. INTRODUCTION

In 2015, Petrov had proposed a scheme for suppression of the collapse in a binary (two-species) Bose-Einstein condensate (BEC) with  $g_{12}^2 > g_{11}g_{22}$ , where  $g_{12}$  is the strength of the interspecies attraction, while  $g_{11}$  and  $g_{22}$  are strengths of the intraspecies self-repulsion [1]. The stabilization of the system against the collapse is provided by the Lee-Huang-Yang (LHY) effect, i.e., corrections to the mean-field BEC dynamics induced by quantum fluctuations [2]. The analysis had predicted the arrest of the collapse and formation of stable quantum droplets (QDs) filled by the ultra-diluted quantum fluid. Following the prediction, QDs have been created in a mixture of two hyperfine atomic states of  $^{39}\text{K}$ , with the quasi-two-dimensional (quasi-2D) [3, 4] and fully 3D [5] shapes, as well as in a heteronuclear mixture of  $^{23}\text{Na}$  and  $^{87}\text{Rb}$  [6] atoms. The use of the LHY effect has also made it possible to create QDs in single-component dipolar bosonic gases of dysprosium [7] and erbium [8] atoms. The analysis has demonstrated that the LHY corrections take different forms in 1D, 2D, and 3D configurations [9].

Studies of QDs have drawn much interest in very different contexts [10–53]. Various phenomena, such as the spin-orbit coupling [54], supersolidity [55, 56], and metastability [57] can be simulated in BECs under the action of the LHY corrections. Further, stable semi-discrete vortex QDs were predicted in arrays of coupled 1D cigar-

shaped traps [58], and the symmetry breaking of QDs has been studied in a dual-core trap [59].

Solitary vortices are often subject to the azimuthal modulational instability that develops faster than the collapse, splitting the vortices into fragments. Therefore, stability conditions for vortex QDs become increasingly stricter with the increase of their winding number, (alias the topological charge). The possibility for the stabilization of vortex modes (matter-wave solitons and QDs) has been revealed by studies of BEC systems under the action of spatially periodic and quasiperiodic lattice potentials [60–72]. Recently, stable QDs in 2D square lattices [73] and ring-shaped QDs with explicit and hidden vorticity in a radially periodic potential [74, 75] have been predicted. In free space, stable 2D matter-wave solitons were predicted in microwave-coupled binary condensates [76].

In dipolar BECs, QDs have been observed in the form of 3D self-bound states. In the 2D geometry, the coherence properties of QDs have been explored in Ref. [77]. In Ref. [78], the ground-state properties and intrinsic excitations of QDs in dipolar BECs have been studied in detail. The previous studies demonstrate that QDs in dipolar BECs feature strong anisotropy of their density profile in the free space, but they do not carry vorticity. In Ref. [79], isotropic vortex QDs with the dipoles polarized parallel to the vortical pivot were constructed and found to be completely unstable. Thus, creating stable vortex QDs in BECs with dipole-dipole interactions (DDI) remains a fundamental problem. Recently, solutions for 2D fundamental QDs in dipolar BEC with the dipoles oriented perpendicular to the system's plane have been produced [80]. Furthermore, Li *et al.* have proved

\*Electronic address: binliu@fosu.edu.cn

†Electronic address: huanboluo@fosu.edu.cn

that dipolar BEC offers a unique possibility to predict stable 2D anisotropic vortex QDs with the vortex axis oriented perpendicular to the polarization of dipoles [81]. Hence, modifying the attractive nonlinearity by introducing DDI is a promising direction for the stabilization of vortex QDs in BEC. The objective of the present work is to demonstrate that the stabilization is also possible with the help of long-range quadrupole-quadrupole interactions (QQI) between particles in BEC. Previously, the formation of solitons in QQI-coupled BEC was addressed in models that did not include the LHY terms [82–84], which made it more difficult to stabilize the self-trapped states in the BEC.

Electric quadrupoles may be built as tightly bound pairs of dipole and antidipoles directed perpendicular to the system's  $(x, y)$  plane, i.e., along the  $z$ -axis. By applying an external gradient electric field along the  $z$ -axis the electric QQI (alias EQQI) can be induced. The potential of the interaction between two electric quadrupoles in this configuration is written in the polar coordinates  $(r, \theta)$  as

$$U_{QQ}^{(\text{elect})}(r, \theta) = \frac{4}{3}Q^2r^{-5} (3 - 5 \cos^2 \theta), \quad (1)$$

where  $Q$  is the quadrupole moment,  $r$  is the distance between the quadrupoles, and  $\theta$  is the angle between the vector connecting the quadrupoles and the line connecting the dipole and antidipole inside the quadrupole. Averaging potentials (1) over the angular range  $0 \leq \theta < 2\pi$  yields the respective mean values:

$$\frac{1}{2\pi} \int_0^{2\pi} U_{QQ}^{(\text{elect})}(r, \theta) d\theta = -2Q^2r^{-5} < 0. \quad (2)$$

According to Eq. (2), the EQQI represent the attractive interaction.

Relatively large electric quadrupole moments are featured by some small molecules [85] and by bound states in the form of alkali diatoms [86]. These particles can be used to create BEC in which EQQI plays an essential role. In Ref. [82], the creation of quadrupolar matter-wave solitons in the 2D free space was predicted, with a conclusion that, in the presence of EQQI, the solitons feature a higher mass and stronger anisotropy than their DDI-maintained counterparts, for the same environmental parameters. Possibilities of building 2D (quasi-) discrete matter-wave solitons composed of quadrupole particles trapped in deep isotropic and anisotropic optical-lattice potentials was demonstrated in Refs. [83] and [84], respectively. In Ref. [87], soliton solutions of the mixed-mode and semi-vortex types were constructed in binary quadrupolar BECs including spin-orbit coupling.

Magnetic quadrupoles can be built as tightly bound dipole-antidipole pairs directed along a particular axis  $(x)$ . They can be polarized parallel to each other by a gradient magnetic field also directed along the  $x$ -axis. The potential of the magnetic quadrupole-quadrupole interactions (MQQI) is

$$U_{QQ}^{(\text{magn})}(r, \theta) = \frac{4}{3}Q^2r^{-5} (3 - 30 \cos^2 \theta + 35 \cos^4 \theta), \quad (3)$$

cf. Eq. (1). Unlike EQQI, which is attractive on the average, for MQQI the mean value of potential (3) corresponds to repulsion:

$$\frac{1}{2\pi} \int_0^{2\pi} U_{QQ}^{(\text{magn})}(r, \theta) d\theta = \frac{3}{2}Q^2r^{-5} > 0, \quad (4)$$

cf. Eq. (2).

In the usual mean-field approximation, which is represented by Gross-Pitaevskii (GP) equation for the single-particle wave function  $\psi$  [88], BEC cannot maintain localized states with the help of MQQI, unless an external trapping potential is used Ref. [89]. However, the above-mentioned proposal to create QDs in BEC by means of the LHY correction to the mean-field approximation [1, 9] suggests a possibility to predict self-trapped objects supported by the QQI. Note that the LHY terms take different forms for different spatial dimensions. In 3D, this term in the corrected GP equation is proportional to  $|\psi|^3\psi$ , with the sign representing self-repulsion [1]. In 2D, the combined mean-field-LHY term is

$$\text{2D local term} = \text{const} \cdot |\psi|^2 \ln(|\psi|^2/n_0) \cdot \psi, \quad (5)$$

where const is a positive coefficient, and  $n_0$  is the equilibrium density [9]. It features the attraction at  $|\psi|^2 < n_0$ , and repulsion at  $|\psi|^2 > n_0$ . Finally, in 1D, the LHY term is proportional to  $-|\psi|\psi$ , with the sing corresponding to the self-attraction, which helps to build solitons and QDs in the effectively one-dimensional condensate [9].

In this work, we produce 2D solutions for self-bound states, including ones with embedded vorticity, in magnetic quadrupolar BEC, taking the corresponding LHY correction into account. Following the original proposal [1, 9] which derived the correction for the two-component BEC, we also address the two-component system. In this connection, it is relevant to stress that the LHY correction to the GP equation for the dipolar BEC has the same form (in particular, being  $\sim |\psi|^3\psi$  in 3D) as in the case of the BEC with contact-only atomic interactions [90, 91]. Accordingly, the same is true for the BEC featuring the long-range MQQI in the combination with the local nonlinearity.

We here consider the 2D model with coordinates  $(x, y)$ , including a gradient magnetic field oriented along the  $x$  direction. This field is induced by a tapered solenoid, as shown schematically in Fig. 1. In this configuration, the MQQI, defined as per Eq. (3), represents self-repulsion, while the local interaction, combining the mean-field and LHY terms according to Eq. (5) may account for attraction. The self-trapping of QDs is achieved through competition between these terms.

Fundamental QDs and quasi-isotropic vortical ones are produced by the analysis presented below. Effects of the

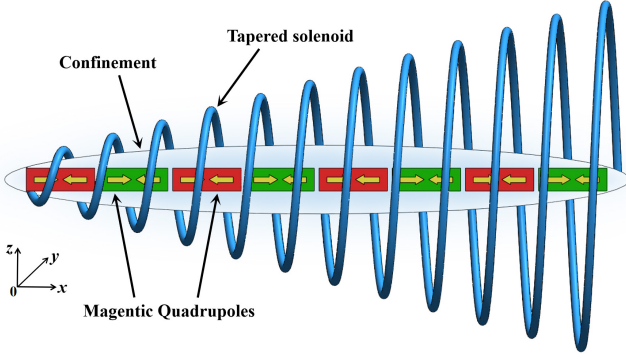


FIG. 1: The system's scheme. Quadrupoles are built as tightly-bound dipole-antidipole pairs, polarized along the  $x$  axis by means of the gradient magnetic field (with the local strength being a linear function of  $x$ ), cf. Ref. [83]. This field can be imposed by the tapered solenoid, as shown in the figure. Red and green rectangles represent two components of the bosonic mixture.

norm and strength of the MQQI are systematically studied. The rest of the paper is structured as follows. The model is introduced in Sec. II. Numerical findings and some analytical estimates are summarized in Sec. III. The dynamics of the QDs are the focus of Sec. IV. The paper is concluded in Sec. V.

## II. THE MODEL

We aim to consider two-component QDs in the magnetic quadrupolar BEC, which is made effectively two-dimensional by the application of strong confinement in the transverse direction. The orientation of individual quadrupoles is fixed as in Fig. 1. The system's dynamics are governed by the coupled GP equations including the LHY correction. In the scaled form, they are written as [81, 90, 91]

$$i\frac{\partial\psi_+}{\partial t} = -\frac{1}{2}\nabla^2\psi_+ + (g_{11}|\psi_+|^2 + g_{12}|\psi_-|^2)\psi_+ + \gamma_{\text{QF}}^{(2\text{D})}\psi_+ [|\psi_+(\mathbf{r})|^2 + |\psi_-(\mathbf{r})|^2] \times \ln [|\psi_+(\mathbf{r})|^2 + |\psi_-(\mathbf{r})|^2] + \kappa\psi_+(\mathbf{r}) \times \iint d\mathbf{r}' R(\mathbf{r}-\mathbf{r}') [|\psi_+(\mathbf{r}')|^2 + |\psi_-(\mathbf{r}')|^2] \quad (6)$$

$$i\frac{\partial\psi_-}{\partial t} = -\frac{1}{2}\nabla^2\psi_- + (g_{22}|\psi_-|^2 + g_{12}|\psi_+|^2)\psi_- + \gamma_{\text{QF}}^{(2\text{D})}\psi_- [|\psi_-(\mathbf{r})|^2 + |\psi_+(\mathbf{r})|^2] \times \ln [|\psi_-(\mathbf{r})|^2 + |\psi_+(\mathbf{r})|^2] + \kappa\psi_-(\mathbf{r}) \times \iint d\mathbf{r}' R(\mathbf{r}-\mathbf{r}') [|\psi_-(\mathbf{r}')|^2 + |\psi_+(\mathbf{r}')|^2] \quad (7)$$

where  $\psi_{\pm}$  are wave functions of the two components,  $\mathbf{r} = \{x, y\}$  is the set of coordinates,  $\nabla^2 = \partial_x^2 + \partial_y^2$ ,  $g_{11,22} > 0$

and  $g_{12} < 0$  are strengths of the contact intra-component repulsion and inter-component attraction, while coefficients  $\gamma_{\text{QF}}^{(2\text{D})}$  and  $\kappa$  represent the LHY correction and MQQI, respectively. The MQQI kernel is

$$R(\mathbf{r}-\mathbf{r}') = \frac{3 - 30\cos^2\theta + 35\cos^4\theta}{[b^2 + (\mathbf{r}-\mathbf{r}')^2]^{5/2}}, \quad (8)$$

cf. Eq. (3), where  $\cos^2\theta = (x-x')^2/(\mathbf{r}-\mathbf{r}')^2$  and  $b$  is the cutoff, which is determined by the thickness of the transverse confinement. By means of scaling, we set  $b \equiv 1$ .

Coefficients  $\gamma_{\text{QF}}^{(2\text{D})}$  can be removed by rescaling,  $t \leftarrow \gamma_{\text{QF}}^{(2\text{D})}t$ ,  $(x, y) \leftarrow \sqrt{\gamma_{\text{QF}}^{(2\text{D})}}(x, y)$ ,  $\kappa \leftarrow \kappa/\gamma_{\text{QF}}^{(2\text{D})}$ . Further, the symmetry constraints,  $\psi_+ = \psi_- = \psi/\sqrt{2}$  and  $g_{11} = g_{22} = -g_{12} \equiv g$ , reduce Eqs. (6,7) to a single equation:

$$i\frac{\partial\psi}{\partial t} = -\frac{1}{2}\nabla^2\psi + \ln(|\psi|^2) \cdot |\psi|^2\psi + \kappa\psi \int R(\mathbf{r}-\mathbf{r}')|\psi(\mathbf{r}')|^2 d\mathbf{r}', \quad (9)$$

where  $\kappa$  remains the single control parameter. Dynamical invariants of Eq. (9) is the total norm,

$$N_{2\text{D}} = \int |\psi(\mathbf{r})|^2 d\mathbf{r}, \quad (10)$$

which is proportional to the number of atoms in the BEC, and the total energy, that includes the mean-field and LHY terms:

$$E = \frac{1}{2} \int [|\nabla\psi|^2 + |\psi|^4 \ln\left(\frac{|\psi|^2}{\sqrt{e}}\right) + \kappa \int R(\mathbf{r}-\mathbf{r}')^2 |\psi(\mathbf{r}')|^2 |\psi(\mathbf{r})|^2 d\mathbf{r}'] d\mathbf{r}. \quad (11)$$

Moving states also conserve the integral momentum,  $\mathbf{P} = i \int \psi \nabla \psi^* d\mathbf{r}$ , where  $*$  stands for the complex conjugate. Strictly speaking, the anisotropy present in Eqs. (8) and (9) breaks the conservation of the angular momentum in the present setting. In fact, the QDs in our system are found to be quasi-isotropic, therefore the angular momentum is approximately conserved.

We look for stationary solutions to Eq. (9), which represents stationary QDs with the chemical potential  $\mu$  in the usual form,

$$\psi(\mathbf{r}, t) = \phi(\mathbf{r}) e^{-i\mu t}, \quad (12)$$

where  $\phi(\mathbf{r})$  is a wave function with is real for fundamental states, and complex for vortex ones. Stationary quasi-isotropic QDs were produced by means of the well-known imaginary-time-propagation (ITP) method [92–94].

### III. STATIONARY SOLUTIONS FOR THE QUANTUM DROPLETS (QDS)

The strength of the MQQI,  $\kappa$ , and the total norm,  $N$ , as used as control parameters in the present analysis. Quasi-isotropic QDs were produced by means of the ITP method, with the ansatz (initial guess)

$$\phi^{(S)}(x, y) = Ar \exp(-\alpha r^2 - iS\theta), \quad (13)$$

where  $\alpha$  and  $A$  are real constants,  $r$  and  $\theta$  are 2D polar coordinates, and  $S$  is vorticity (topological charge, alias winding number). Further, stability of the stationary QD states was verified by direct simulations of the perturbed evolution (run by dint of the fast-Fourier-transform algorithm), adding random noise at the 1% amplitude level to the input. To this end, the input was taken as  $\psi = [1 + \varepsilon' f(x, y)] \cdot \phi^{(S)}(x, y)$ , where,  $\varepsilon' = 1\%$  and  $f(x, y)$  is a random function with the value range  $[0, 1]$ , which can be generated by the standard “rand” function.

#### A. Fundamental QDs

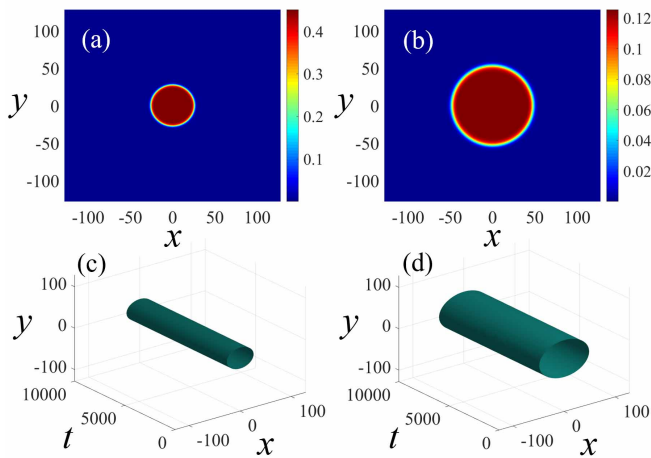


FIG. 2: Typical examples of stable quasi-isotropic fundamental quantum droplets (QDs) produced by input (13) with  $S = 0$ . Panels (a) and (b) display the density profiles of the QDs with  $(N, \kappa) = (1000, 0.1)$  and  $(1000, 0.5)$ . (c) and (d): The perturbed evolution of the QDs from (a) and (b), produced by simulations of Eq. (9) with the 1% random noise added to the input.

Typical examples of numerically constructed stable quasi-isotropic fundamental QDs with  $S = 0$  are displayed in Fig. 2. The parameters are  $(N, \kappa) = (1000, 0.1)$  in (a) and  $(1000, 0.5)$  in (b). The stability of these QDs was confirmed by direct simulations of their perturbed evolution, as shown in Figs. 2(c,d). Similar to QDs in binary bosonic gases with contact-only interactions, the

quasi-isotropic QDs in the quadrupolar BEC generally feature flat-top density profiles. In this case, one can apply the Thomas-Fermi (TF) approximation, neglecting the gradient term in energy (11). The corresponding approximation yields

$$E_{\text{TF}} = \frac{1}{2} \left( \kappa \varepsilon n^2 + n^2 \ln \left( \frac{n}{\sqrt{e}} \right) \right) A_S, \quad (14)$$

where  $n = |\psi|^2$ ,  $A_S = N/n$  is the effective area of the flat-top QD, and

$$\varepsilon \equiv \int d\mathbf{r} R(\mathbf{r}) \approx 3.2, \quad (15)$$

with  $R(\mathbf{r})$  taken as per Eq. (8), is an effective measure of the repulsive nonlocality. Then, one can obtain the equilibrium density  $n_e$  and the effective area  $A_S$  of the quasi-isotropic QD from the energy-minimum condition  $dE/dn = 0$ , which yields

$$A_S = N e^{(\kappa \varepsilon + 1/2)}, \quad (16)$$

$$n_e = e^{-(\kappa \varepsilon + 1/2)}. \quad (17)$$

The chemical potential corresponding to the equilibrium density (17) is

$$\mu_e = \kappa \varepsilon n_e + n_e \ln n_e. \quad (18)$$

Further, as a characteristics of the QDs, we define their effective area:

$$A_{\text{eff}} = \frac{\left( \int |\psi|^2 d\mathbf{r} \right)^2}{\int |\psi|^4 d\mathbf{r}}. \quad (19)$$

Comparing the results for  $\kappa = 0.1$  and  $\kappa = 0.5$  in Fig. 2, we conclude that the effective area is larger in the latter case, as is also seen in Fig. 3(a<sub>1</sub>).

For the fixed norm, the dependence of the effective area  $A_{\text{eff}}$  on the MQQI strength  $\kappa$  is shown in Fig. 3(a<sub>1</sub>), which indicates that the effective area exponentially grows the increase of  $\kappa$ . Here, the solid blue and dotted red lines show, respectively, results of the numerical simulations and the analytical results, produced by Eq. (16), the two curves being almost identical.

Next, we show the peak density,  $I_p$  ( $I_p = |\psi|_{\text{max}}^2$ ), and the chemical potential  $\mu$  of the stable quasi-isotropic QDs as functions of the MQQI strength  $\kappa$  in Figs. 3(a<sub>2</sub>) and (a<sub>3</sub>), respectively. Figure 3(a<sub>2</sub>) shows that  $I_p$  decreases with  $\kappa$ , which is also in agreement with Eq. (17), in which the peak density decays exponentially with the increase of the MQQI strength.

In Figs. 3(b<sub>1</sub>) - 3(b<sub>3</sub>), we fix the MQQI strength  $\kappa$ , considering the dependence of the effective area  $A_{\text{eff}}$ , peak density  $I_p$ , and chemical potential  $\mu$  on the total norm  $N$ . Similar to the 2D anisotropic QDs in dipolar BECs, the effective area of the quasi-isotropic QDs

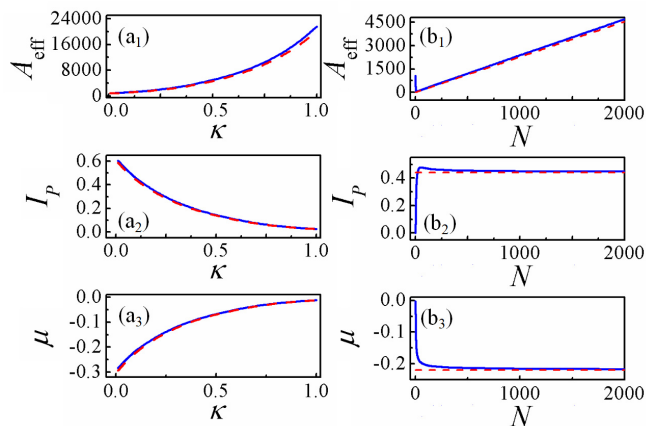


FIG. 3: The first column (a<sub>1</sub>-a<sub>3</sub>): the effective area ( $A_{\text{eff}}$ ), peak density ( $I_p$ ), and chemical potential ( $\mu$ ) of the fundamental quasi-isotropic QDs as functions of the strength of  $\kappa$  with the norm  $N = 500$ . The second column (b<sub>1</sub>-b<sub>3</sub>): the dependence of  $A_{\text{eff}}$ ,  $I_p$  and  $\mu$  on the norm,  $N$ , with  $\kappa = 0.1$ . Here, the solid blue line shows the numerical simulation results, and the dotted red line show the analytical approximations, see Eq. (16), (17), and (18), for  $A_{\text{eff}}$ ,  $I_p$  and  $\mu$ , respectively.

grows linearly with the increase of the total norm, see Eq. (16), which is a natural feature of flat-top modes. In Fig. 3(b<sub>2</sub>), the peak density saturates at  $I_p \approx 0.448$ , if  $N$  is sufficiently large, which corroborates that the superfluid filling the QDs is incompressible, as demonstrated first in Ref. [1]. According to Eq. (17), the theoretical prediction equilibrium density is about 0.440, which is very close to the numerical results [see the red dashed line in Fig. 3(b<sub>2</sub>)]. The  $\mu(N)$  curves in Fig. 3(b<sub>3</sub>) feature a negative slope, i.e.,  $d\mu/dN < 0$ , which satisfies the Vakhitov-Kokolov (VK) criterion [95], which is a necessary stability condition for self-trapped modes maintained by a self-attractive nonlinearity. Figure 3(b<sub>3</sub>) shows that the chemical potential saturates at  $\mu \approx -0.217$  when the norm is large. The TF-predicted value given by Eq. (18) is  $\mu_e \approx -0.220$  [see the red dashed line in Fig. 3(b<sub>3</sub>)]. As shown in Fig. 3, all the numerical results agree well with the analytical predictions provided by Eqs. (16), (17) and (18).

## B. QDs with embedded vorticity

The present system maintains stable vortex QDs (VQDs) too. A typical example of a numerically constructed one with winding number  $S = 1$ , produced by input (13) with  $S = 1$ , is displayed in Fig. 4, for  $N = 1000$ , and  $\kappa = 0.1$ . The stability of these VQDs was confirmed by direct simulations of its perturbed evolution, see Fig. 4(c), where 1% random noise is added to the input.

To systematically study characteristics of the VQD families, we define their aspect ratio and average angular

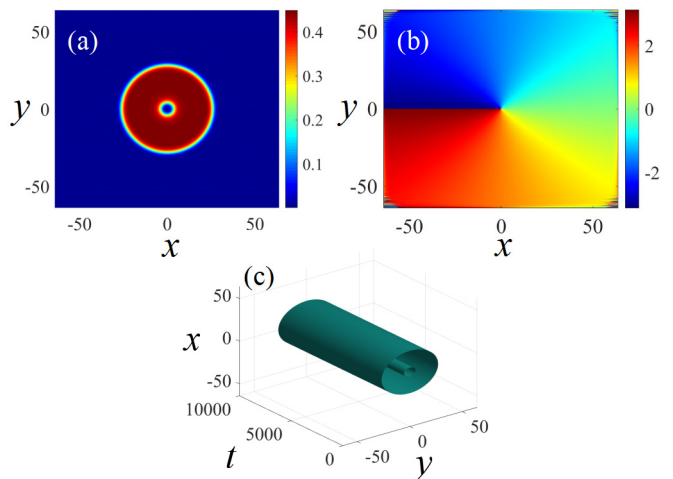


FIG. 4: (a) and (b): The density and phase patterns of a stable quasi-isotropic VQD (vortex QD) produced by Eq. (13) with winding number  $S = 1$  and  $(N, \kappa) = (1000, 0.1)$ . (c) Simulations of the perturbed evolution of the VQDs shown in panel (a) with 1% random noise added to the input.

momentum as follows:

$$A_l = \frac{W_y}{W_x}, \quad (20)$$

$$\bar{L}_z = \int \frac{\phi^* \hat{L}_z \phi}{N} d\mathbf{r}, \quad (21)$$

where  $W_{x,y}$  and  $\bar{L}_z$  represent the effective lengths of the VQDs in the  $x/y$ -direction, and angular momentum operators, respectively:

$$W_x \equiv \frac{\left( \int |\phi(x, y=0)|^2 dx \right)^2}{\int |(x, y=0)|^4 dx}, \quad (22)$$

$$W_y \equiv \frac{\left( \int |\phi(x=0, y)|^2 dy \right)^2}{\int |(x=0, y)|^4 dy}, \quad (23)$$

$$\hat{L}_z = -i(x\partial_y - y\partial_x). \quad (24)$$

In particular,  $A_l < 1$  indicates that the VQDs manifest anisotropy with the elongation along the  $x$ -direction, while  $A_l = 1$  implies their isotropy [81].

The aspect ratio  $A_l$  and average angular momentum  $\bar{L}_z$  of stable VQDs with  $N = 500$ , defined as per Eqs. (20)-(24), are displayed in Figs. 5(a<sub>1</sub>) and 5(a<sub>2</sub>), respectively, as functions of the MQQI strength  $\kappa$ , varying in interval  $0 < \kappa < 1$ . Note that, according to Fig. 3(a<sub>1</sub>), the effective area of QDs exponentially grows with the increase of  $\kappa$ , making the calculations more difficult. For this reason, we here present the results for  $\kappa < 1$ . Figures 5(b<sub>1</sub>) and (b<sub>2</sub>) display the VQD characteristics  $A_l$  and  $\bar{L}_z$  as functions of the norm  $N$ , with  $\kappa = 0.1$ . In panels 5(a<sub>1</sub>), the aspect ratio attains a maximum value 1.1742 and approaches 1.0677 at  $\kappa \rightarrow 1$ . Figure 5(a<sub>2</sub>) depicts the respective orbital momentum, whose average

value is 0.9955. In panels 5(b<sub>1</sub>) and (b<sub>2</sub>), the aspect ratio and orbital momentum have values of  $A_l \approx 1.0921$  and  $\bar{L}_z \approx 0.9957$ , respectively. These findings indicate that the system with the repulsive MQQI maintains stable quasi-isotropic VQDs, whose aspect ratio is slightly larger than 1. In this connection, it is relevant to mention that for the fundamental QD modes considered above, values of the aspect ratio are also approximate equal to 1, as the density distribution in those modes seem to be axisymmetric (isotropic).

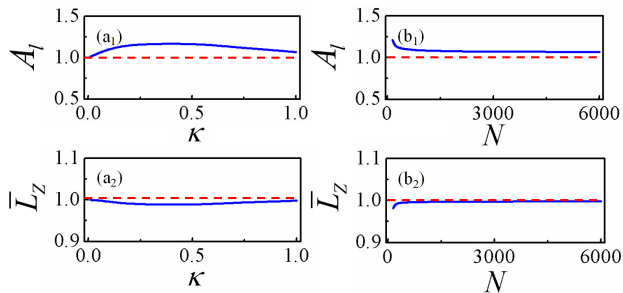


FIG. 5: Panels (a<sub>1</sub>) and (a<sub>2</sub>) display the aspect ratio  $A_l$  and average angular momentum  $\bar{L}_z$  of stable quasi-isotropic VQDs with  $N = 500$ , respectively, as functions of the MQQI strength  $\kappa$ . Panels (b<sub>1</sub>) and (b<sub>2</sub>) display the values,  $(A_l, \bar{L}_z)$ , for VQDs as functions of the norm  $N$ , with  $\kappa = 0.1$ . The red dashed line designates the unit levels.

Simulations of in elastic collisions between moving stable VQDs with  $S = 1$  (see Fig. 10 below) demonstrate that they may merge into a single breather with angular momentum (21) close to  $\bar{L}_z = 2$ . This fact suggests that stable VQDs with  $S = 2$  may exist too. A typical example of such a vortex state, produced by input Eq. (13) with  $S = 2$ , are displayed in Fig. 6, with the same parameters as in Fig. 4. The respective values given by Eqs. (20) and (21) for this double VQD are  $A_l = 0.9718$  and  $\bar{L}_z \approx 1.9824$  at  $t = 10000$ .

The family of VQDs with  $S = 2$  are characterized by dependences of their chemical potential  $\mu$  on  $\kappa$  and  $N$ , as shown in Figs. 7(a) and (b). Next, we fix the characteristic value of the MQQI strength,  $\kappa = 0.3$ , to study a relation between the chemical potential  $\mu$  of VQDs with  $S = 2$  and their norm  $N$ . Figure 7(a) shows that the  $\mu(N)$  curve has a negative slope, satisfying the VK criterion. It is worthy to note that, for the current fixed values  $S = 2$  and  $\kappa = 0.3$ , the VQDs are stable in a finite interval,  $950 < N < 1250$ , see the red line in Fig. 7(a), while the black dotted segments of the curves represent unstable states, for the same parameters. In Fig. 7(b), with  $N = 1000$ , the stable VQDs with  $S = 2$  populate the area of  $\kappa < 0.45$ .

We have also constructed VQD states with higher vorticities,  $S \geq 3$ , as shown in Fig. 8. Typical examples of QDs with  $S = 3$  and  $S = 4$ , with parameters  $(N, \kappa) = (5000, 0.1)$  and  $(N, \kappa) = (15000, 0.1)$ , are displayed in Figs. 8(a<sub>1</sub>) - (a<sub>5</sub>) and 8(b<sub>1</sub>) - (b<sub>5</sub>), respectively.

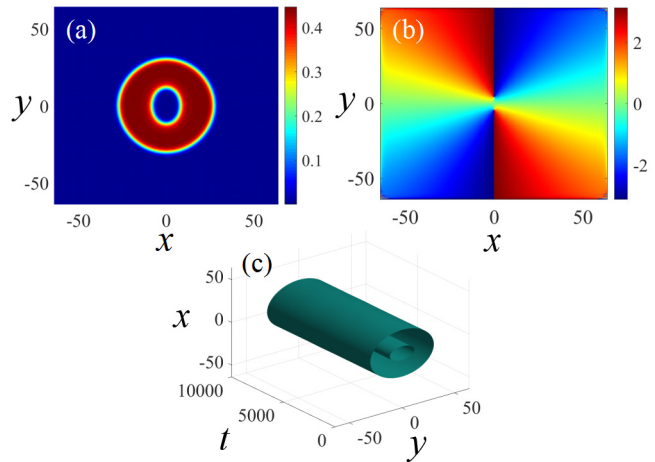


FIG. 6: Panels (a) and (b): The density and phase patterns of a stable VQD with winding number  $S = 2$ . The other parameters are the same as in Fig. 4. (c) Simulations of the perturbed evolution of the VQD shown in panels (a) and (b), with 1% random noise added to the input.

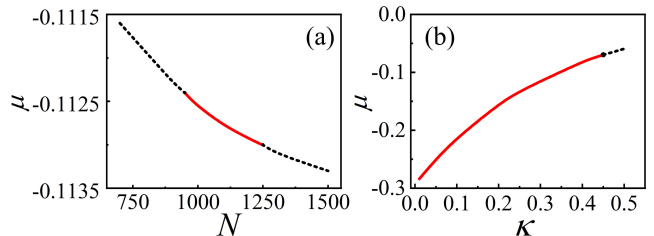


FIG. 7: (a) and (b): The chemical potential of the stable VQDs with  $S = 2$  versus  $N$  (at  $\kappa = 0.3$ ) and  $\kappa$  (at  $N = 1000$ ), respectively. The red solid and black dotted segments of the curves represent, respectively, stable and unstable states.

Figures 8(a<sub>1</sub>,b<sub>1</sub>) and (a<sub>5</sub>,b<sub>5</sub>), respectively, display the initial ( $t = 0$ ) and final ( $t = 10000$ ) phase patterns of for  $S = 3$  and 4. Figures 8(a<sub>2</sub>) - (a<sub>4</sub>) and 8(b<sub>2</sub>) - (b<sub>4</sub>) show the density patterns at  $t = 0, 5000$ , and 10000. The simulations demonstrate that those QDs are stable and feature quasi-isotropic shapes. According to Eq. (20), we have found  $A_l \approx 1.0308$  in Fig. 8(a<sub>4</sub>) and  $A_l \approx 1.1338$  in Fig. 8(b<sub>4</sub>). Further, according to Eq. (21), we have calculated the average angular momentum of these QDs at  $t = 10000$ ,  $\bar{L}_z \approx 2.9633$  in Fig. 8(a<sub>4</sub>) and  $\bar{L}_z \approx 3.8869$  in Fig. 8(b<sub>4</sub>), which exhibit a small deviation from the corresponding initial values of the angular momentum.

#### IV. DYNAMICS OF THE QUANTUM DROPLETS (QDS)

It is well known that stable QDs in binary BECs can be set in motion by opposite kicks with magnitude  $\pm\eta$  applied along the  $x$ - or  $y$ -direction, which suggests to consider collisions between two QDs moving in the op-

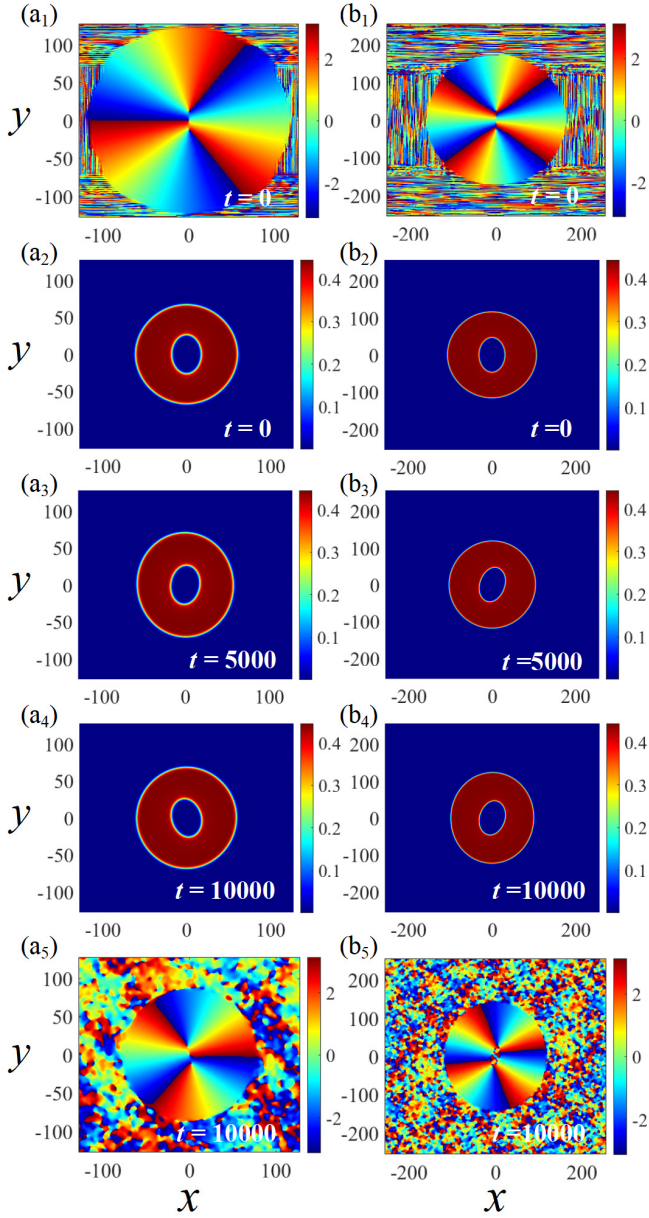


FIG. 8: Typical examples of quasi-isotropic VQDs with  $(N, S) = (5000, 3)$  and  $(N, S) = (15000, 4)$ .  $(a_1, b_1)$  and  $(a_5, b_5)$  display the VQD phase patterns at  $t = 0$  and  $t = 10000$ , respectively. Panels  $(a_2-a_4)$  and  $(b_2-b_4)$  show the density patterns of the VQDs at  $t = 0, 5000$ , and  $10000$ , respectively.

posite directions [96, 97]. Here, we address the collisions between the QDs moving in the  $x$  direction. The corresponding initial states are constructed as

$$\psi(x, y, t = 0) = \phi(x - x_0, y) e^{-i\eta x} + \phi(x + x_0, y) e^{i\eta x}, \quad (25)$$

where  $\phi(x \pm x_0, y)$  represents the stationary quasi-isotropic QDs initially centered at  $x = \mp x_0$ . It is necessary to choose  $x_0$  large enough so that the two QDs are initially placed far from each other, avoiding any overlap.

### A. Collisions between fundamental QDs

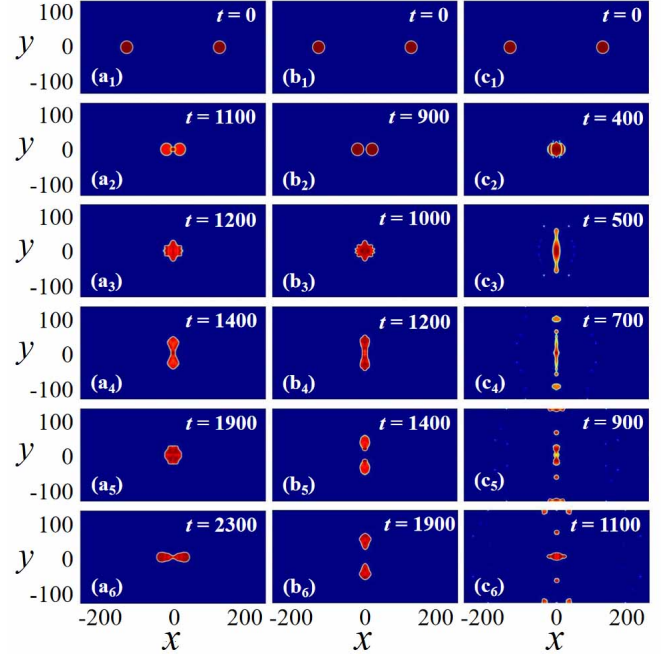


FIG. 9: Examples of collisions between moving quasi-isotropic fundamental QDs, produced by input (25) with  $x_0 = 128$ . Initial parameters of the QDs are  $(N, \kappa) = (500, 0.05)$ .  $(a_1) - (a_6)$ : A strongly inelastic collision of two QDs, set in motion by kicks  $\pm 0.1$ .  $(b_1) - (b_6)$ : A collision initiated by kicks  $\pm 0.12$ .  $(c_1) - (c_6)$ : An inelastic collision in the case of strong kicks,  $\pm 0.3$ , which implies the collision with a large relative velocity.

First, we consider the collisions between moving fundamental QDs ( $S = 0$ ). In Ref. [59], where collisions between two-component QDs have been considered in the model with contact interactions, the simulations demonstrated a trend to inelastic outcomes produced by the collisions between QDs in the in-phase configuration. In Ref. [43], the collisional dynamics has been studied for two symmetric QDs with equal intraspecies scattering lengths and equal densities of both components. In Ref. [81], the collisions between moving 2D anisotropic vortex QDs have been studied, demonstrating the formation of bound states with a vortex-antivortex-vortex structure.

We have produced typical results for the collisions, produced by input (25) with  $(N, x_0, \kappa) = (500, 128, 0.05)$ . The results are shown in Fig. 9. Figures 9(a<sub>1</sub>) - (a<sub>6</sub>) show the result of the strongly inelastic collision between moving QDs set in motion by kicks  $\pm 0.1$ . The result is fusion of the two fundamental QDs in a quadrupole breather. It stretches periodically in the  $x$  and  $y$  directions, which somewhat resembles dynamics which may be featured by a liquid drop [43]. When the initial kicks increase to  $\pm 0.12$ , quasi-elastic outcomes of the collision are observed. In this case, Figs. 9(b<sub>1</sub>) - (b<sub>6</sub>) show that the colliding droplets separate into another pair of droplets, slowly moving in the perpendicular direction,

i.e., the collision leads to the deflection of the direction of motion by  $90^\circ$ . Similar results were mentioned in Refs. [43, 80]. When the norm is fixed, the outcome of the collision is mainly determined by the velocity, i.e., by kick  $\eta$  [43, 59, 98]. If the collision speed exceeds a critical value, an inelastic collision takes place. A typical example of an inelastic collision of two quasi-isotropic fundamental QDs is shown in Figs. 9(c<sub>1</sub>) - (c<sub>6</sub>). After the collision, they split into several fragments. Note that the norm and the MQQI strength (both of which affect the QD's size) also affects the outcome of the collision. We do not consider these effects in detail here.

### B. Collision between moving vortex quantum droplets (VQDs)

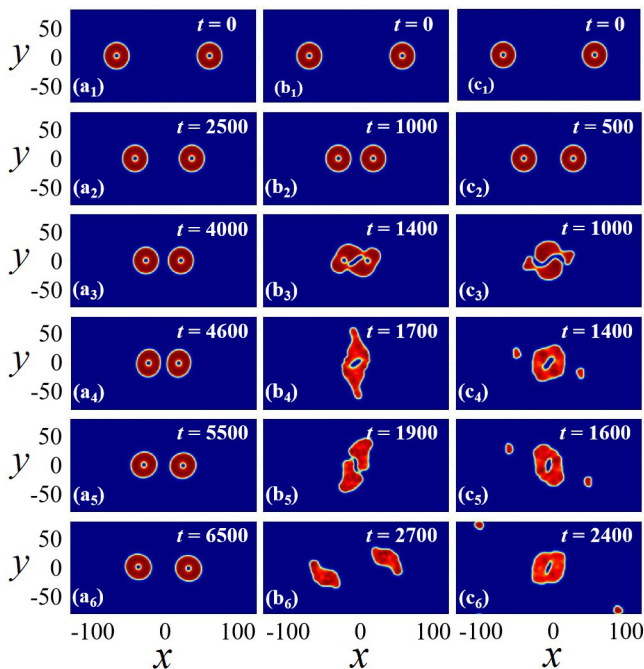


FIG. 10: Several typical examples of collisions between moving quasi-isotropic vortex quantum droplets (VQDs), by inputting Eq. (25) with  $x_0 = 64$ , which are selected with  $(N, \kappa, S) = (500, 0.05, 1)$ . (a<sub>1</sub>) - (a<sub>6</sub>) Contactless collision with the kick  $\eta = 0.01$ . (b<sub>1</sub>) - (b<sub>6</sub>) Collision with the kick  $\eta = 0.04$ . (c<sub>1</sub>) - (c<sub>6</sub>) Collision with the kick,  $\eta = 0.06$ .

Next, we consider collisions between moving VQDs. For input Eq. (25) with  $(N, x_0, \kappa, S) = (500, 64, 0.05, 1)$ , several typical outcomes of the collision are presented in Fig. 10. In Figs. 10(a<sub>1</sub>) - (a<sub>6</sub>), the collision with a small relative speed, initiated by small kicks (here, they are  $\pm 0.01$ ), the two VQDs bounce back, keeping their original vorticities, as a result of the contactless collision. According to Eq. (21), angular momenta of the two droplets in Fig. 10(a<sub>6</sub>) are  $\bar{L}_{z,\text{right}} = \bar{L}_{z,\text{left}} \approx 1.005$ . It is worth noting that the mutual rebound does not occur in the case of the collision of fundamental QDs, as seen in

Fig. 9. By gradually increasing the kicks to  $\pm 0.04$ , the colliding VQDs merge and eventually split into a couple of non-vortical fragments, see Fig. 10(b<sub>1</sub>) - (b<sub>6</sub>). The simulations demonstrate a trend to merger of the colliding VQDs into a vortex breather. In particular, this outcome, corresponding to the initial kicks  $\pm 0.06$ , is observed in Figs. 10(c<sub>1</sub>) - 10(c<sub>6</sub>). The emerging breather absorbs 86.34% of the total norm in Fig. 10(c<sub>6</sub>). The angular momentum of the breather is  $\bar{L}_z \approx 1.6860$ , which is relatively close to 2. The VQDs being quasi-isotropic, the average angular momentum is approximately conserved, as mentioned above. This result suggests the existence of stable VQDs with vorticity  $S = 2$ . As demonstrated above, stable stationary VQDs with  $S = 2$  are indeed available.

## V. CONCLUSION

The purpose of this work is to establish the stability and characteristics of 2D quasi-isotropic QDs (quantum droplets) in magnetic quadrupolar BECs. The system is modeled by the coupled GP including the LHY (Lee-Huang-Yang) terms, which represent the correction to the mean field theory produced by quantum fluctuations. Stable quasi-isotropic QDs of the fundamental and vortex types (with topological charges  $S \leq 4$ ) have been produced by means of imaginary-time simulations. The effect of the norm and strength of the MQQI (magnetic quadrupole-quadrupole interactions),  $\kappa$ , on the QDs were studied in detail. It was found that the effective area increases with an increase of  $\kappa$ . For stable QDs, the dependence between the chemical potential and total norm obeys the VK (Vakhitov-Kolokolov) criterion. The dependence of the effective area and peak density of the QDs on  $\kappa$  and norm  $N$  have been studied too. The results of the numerical simulation are consistent with the analytical predictions produced by the TF (Thomas-Fermi) approximation. Collisions between moving QDs have been also studied systematically, for the fundamental and vortex droplets alike.

The present analysis can be extended further. In particular, it is not clear if essentially anisotropic QDs, especially higher-order vortical ones, can exist in the model. A challenging option is to seek for stable vortex QDs in the full 3D setting with MQQI.

## VI. ACKNOWLEDGMENTS

This work was supported by the National Natural Science Foundation of China through grants Nos. 12274077 and 11905032, the Natural Science Foundation of Guangdong province through grant No. 2021A1515010214, the Guangdong Basic and Applied Basic Research Foundation through grants Nos. 2019A1515110924 and 2021A1515111015, the Research Fund of the Guangdong-Hong Kong-Macao Joint Laboratory for Intelligent

Micro-Nano Optoelectronic Technology through grant No. 2020B1212030010, and Israel Science Foundation

through Grant No. 1695/22.

- 
- [1] D. S. Petrov, Quantum mechanical stabilization of a collapsing Bose-Bose mixture, *Phys. Rev. Lett.* **115**, 155302 (2015).
- [2] T. D. Lee, K. S. Huang, and C. N. Yang, Eigenvalues and eigenfunctions of a Bose system of hard spheres and its lowtemperature properties, *Phys. Rev.* **106**, 1135 (1957).
- [3] C. R. Cabrera, L. Tanzi, J. Sanz, B. Naylor, P. Thomas, P. Cheiney, and L. Tarruell, Quantum liquid droplets in a mixture of Bose-Einstein condensates, *Science* **359**, 301 (2017).
- [4] P. Cheiney, C. R. Cabrera, J. Sanz, B. Naylor, L. Tanzi, and L. Tarruell, Bright soliton to quantum droplet transition in a mixture of Bose-Einstein condensates, *Phys. Rev. Lett.* **120**, 135301 (2018).
- [5] G. Semeghini, G. Ferioli, L. Masi, C. Mazzinghi, L. Wolswijk, F. Minardi, M. Modugno, G. Modugno, M. Inguscio, and M. Fattori, Self-bound quantum droplets of atomic mixtures in free space, *Phys. Rev. Lett.* **120**, 235301 (2018).
- [6] Z. Guo, F. Jia, L. Li, Y. Ma, J. M. Hutson, X. Cui, and D. Wang, Lee-Huang-Yang effects in the ultracold mixture of  $^{23}\text{Na}$  and  $^{87}\text{Rb}$  with attractive interspecies interactions, *Phys. Rev. Res.* **3**, 033247 (2021).
- [7] M. Schmitt, M. Wenzel, F. Böttcher, I. Ferrier-Barbut, and T. Pfau, Self-bound droplets of a dilute magnetic quantum liquid, *Nature (London)* **539**, 259 (2016).
- [8] L. Chomaz, S. Baier, D. Petter, M. J. Mark, F. Wächtler, L. Santos, and F. Ferlaino, Quantum-fluctuation-driven crossover from a dilute Bose-Einstein condensate to a macrodroplet in a dipolar quantum fluid, *Phys. Rev. X* **6**, 041039 (2016).
- [9] D. S. Petrov and G. E. Astrakharchik, Ultradilute lowdimensional liquids, *Phys. Rev. Lett.* **117**, 100401 (2016).
- [10] L. Lavoine, and T. Bourdel, Beyond-mean-field crossover from one dimension to three dimensions in quantum droplets of binary mixtures, *Phys. Rev. A* **103**, 033312 (2021).
- [11] I. Ferrier-Barbut, M. Wenzel, F. Böttcher, T. Langen, M. Isoard, S. Stringari, and T. Pfau, Scissors mode of dipolar quantum droplets of dysprosium atoms, *Phys. Rev. Lett.* **120**, 160402 (2018).
- [12] A. Boudjemâa, Fluctuations and quantum self-bound droplets in a dipolar Bose-Bose mixture, *Phys. Rev. A* **98**, 033612 (2018).
- [13] H. Hu, and X. Liu, Microscopic derivation of the extended Gross-Pitaevskii equation for quantum droplets in binary Bose mixtures, *Phys. Rev. A* **102**, 043302 (2020).
- [14] M. Pylak, F. Gampel, M. Płodzień, and M. Gajda, Manifestation of relative phase in dynamics of two interacting Bose-Bose droplets, *Phys. Rev. Res.* **4**, 013168 (2022).
- [15] L. Parisi, and S. Giorgini, Quantum droplets in one-dimensional Bose mixtures: A quantum Monte Carlo study, *Phys. Rev. A* **102**, 023318 (2020).
- [16] L. Dong, D. Liu, Z. Du, K. Shi and W. Qin, Bistable multipole quantum droplets in binary Bose-Einstein condensates, *Phys. Rev. A* **105**, 033321 (2022)
- [17] P. Zin, M. Pylak, and M. Gajda, Revisiting a stability problem of two-component quantum droplets, *Phys. Rev. A* **103**, 013312 (2021).
- [18] S. R. Otajonov, E. N. Tsoy, and F. Kh. Abdullaev, Variational approximation for two-dimensional quantum droplets, *Phys. Rev. E* **102**, 062217 (2020).
- [19] M. Tylutki, G. E. Astrakharchik, B. A. Malomed, and D. S. Petrov, Collective excitations of a one-dimensional quantum droplet, *Phys. Rev. A* **101**, 051601(R) (2020).
- [20] Z. Luo, W. Pang, B. Liu, Y. Li, and B. A. Malomed, A new form of liquid matter: quantum droplets, *Front. Phys.* **16**, 32201 (2021).
- [21] X. Cui, Spin-orbit-coupling-induced quantum droplet in ultracold Bose-Fermi mixtures, *Phys. Rev. A* **98** 023630 (2018).
- [22] Y. Wang, L. Guo, S. Yi and T. Shi, Theory for self-bound states of dipolar Bose-Einstein condensates, *Phys. Rev. Res.* **2**, 043074 (2020).
- [23] L. Dong and Y. V. Kartashov, Rotating multidimensional quantum droplets, *Phys. Rev. Lett.* **126**, 244101 (2021).
- [24] H. Huang, H. Wang, M. Chen, C. S. Lim and K. Wong, Binary-vortex quantum droplets, *Chaos, Solitons and Fractals* **158**, 112079 (2022).
- [25] M. Guo and T. Pfau, A new state of matter of quantum droplets, *Front. Phys.* **16**, 32202 (2021).
- [26] B. A. Malomed, The family of quantum droplets keeps expanding, *Front. Phys.* **16**, 22504 (2021).
- [27] S. Xu, Y. Lei, J. Du, Y. Zhao, R. Hua and J. Zeng, Three-dimensional quantum droplets in spin-orbit-coupled Bose-Einstein condensates, *Chaos, Solitons and Fractals* **164**, 112665 (2022).
- [28] Z. Zhou, Y. Shi, F. Ye, H. Chen, S. Tang, H. Deng and H. Zhong, Self-bound states induced by the Lee-Huang-Yang effect in non-PT-symmetric complex potentials, *Nonlinear Dyn.* **110**, 3769 (2022).
- [29] Z. Zhou, Y. Shi, S. Tang, H. Deng, H. Wang, X. He and H. Zhong, Controllable dissipative quantum droplets in one-dimensional optical lattices, *Chaos, Solitons and Fractals* **150**, 111193 (2021).
- [30] Y. V. Kartashov, V. M. Lashkin, M. Modugno and L. Torner, Spinor-induced instability of kinks, holes and quantum droplets, *New J. Phys.* **24**, 073012 (2022).
- [31] P. Zin, M. Pylak and M. Gajda, Zero-energy modes of two-component Bose-Bose droplets, *New J. Phys.* **23**, 033022 (2021).
- [32] V. Cikojević, L. V. Markić and J. Boronat, Finite-range effects in ultradilute quantum drops, *New J. Phys.* **22**, 053045 (2020).
- [33] A. Cidrim, L. Salasnich and T. Macrì, Soliton trains after interaction quenches in Bose mixtures, *New J. Phys.* **23**, 023022 (2021).
- [34] T. Karpiuk, M. Gajda and M. Brewczyk, Bistability of Bose-Fermi mixtures, *New J. Phys.* **22**, 103025 (2020).
- [35] F. Zhang and L. Yin, Phonon stability of quantum droplets in dipolar Bose gases, *Chin. Phys. Lett.* **39**, 060301 (2022).
- [36] J. Wang, J. Pan, X. Cui and W. Yi, Quantum droplets in a mixture of Bose-Fermi superfluids, *Chin. Phys. Lett.*

- 37**, 076701 (2020).
- [37] J. Wang, X. J. Liu and H. Hu, Ultradilute self-bound quantum droplets in Bose-Bose mixtures at finite temperature, *Chin. Phys. B* **30**, 010306 (2021).
- [38] G. Ferioli, G. Semeghini, L. Masi, G. Giusti, G. Modugno, M. Inguscio, A. Gallemí, A. Recati, and M. Fattori, Collisions of self-bound quantum droplets, *Phys. Rev. Lett.* **122**, 090401 (2019).
- [39] F. Zhao, Z. Yan, X. Cai, C. Li, G. Chen, H. He, B. Liu, and Y. Li, Discrete quantum droplets in one-dimensional optical lattices, *Chaos, Solitons and Fractals*, **152**, 111313 (2021).
- [40] F. Böttcher, J. N. Schmidt, J. Hertkorn, K. S. H. Ng, S. D. Graham, M. Guo, T. Langen, and T. Pfau, New states of matter with fine-tuned interactions: Quantum droplets and dipolar supersolids, *Rep. Prog. Phys.* **84**, 012403 (2021)
- [41] C. D’Errico, A. Burchianti, M. Prevedelli, L. Salasnich, F. Ancilotto, M. Modugno, F. Minardi, and C. Fort, Observation of quantum droplets in a heteronuclear bosonic mixture, *Phys. Rev. Res.* **1**, 033155 (2019).
- [42] I. Ferrier-Barbut, M. Schmitt, M. Wenzel, H. Kadau and T. Pfau, Liquid quantum droplets of ultracold magnetic atoms, *J. Phys. B: At. Mol. Opt. Phys.* **49**, 214004 (2016).
- [43] Y. Hu, Y. Fei, X. Chen, and Y. Zhang, Collisional dynamics of symmetric two-dimensional quantum droplets, *Front. Phys.* **17**, 61505 (2022).
- [44] Y. Zhang, V. Walther and T. Pohl, Long-range interactions and symmetry breaking in quantum gases through optical feedback, *Phys. Rev. Lett.* **121**, 073604 (2018).
- [45] B. Dong, Y. Zhang and X. Zhang, Quantum droplets with topological textures in a dipolar condensate, *Optik* **273**, 170484 (2023).
- [46] Y. Zhang, V. Walther and T. Pohl, Self-bound droplet clusters in laser-driven Bose-Einstein condensates, *Phys. Rev. A* **103**, 023308 (2021).
- [47] Y. Xiong and L. Yin, Self-Bound Quantum Droplet with Internal Stripe Structure in 1D Spin-Orbit-Coupled Bose Gas, *Chin. Phys. Lett.* **38**, 070301 (2021).
- [48] J. Chen and J. Zeng, One-dimensional quantum droplets under space-periodic nonlinear management, *Results Phys.* **21**, 103781 (2021).
- [49] Y. Ma, C. Peng and X. Cui, Borromean droplet in three-component ultracold Bose gases, *Phys. Rev. Lett.* **127**, 043002 (2021).
- [50] X. Cui and Y. Ma, Droplet under confinement: Competition and coexistence with a soliton bound state, *Phys. Rev. Res.* **3**, L012027 (2021).
- [51] S. Xu, Y. Lei, J. Du, Y. Zhao, R. Hua and J. Zeng, Three-dimensional quantum droplets in spin-orbit-coupled Bose-Einstein condensates, *Chaos Solitons Fractals* **164** 112665 (2022).
- [52] Z. Zhou, X. Yu, Y. Zhou and H. Zhong, Dynamics of quantum droplets in a one-dimensional optical lattice, *Commun Nonlinear Sci Numer Simul* **78**, 104881 (2019).
- [53] R. Schützhold, M. Uhlmann, Y. Xu, and U. R. Fischer, Mean-field expansion in Bose-Einstein condensates with finite-range interactions, *Int. J. Mod. Phys. B* **20**, 3555 (2006).
- [54] Y. Li, Z. Luo, Y. Liu, Z. Chen, C. Huang, S. Fu, H. Tan and B. A. Malomed, Two-dimensional solitons and quantum droplets supported by competing self-and cross-interactions in spin-orbit-coupled condensates, *New J. Phys.* **19**, 113043 (2017).
- [55] Y. Zhang, T. Pohl and F. Maucher, Phases of supersolids in confined dipolar Bose-Einstein condensates, *Phys. Rev. A* **104**, 013310 (2021).
- [56] F. Böttcher, J. Schmidt, M. Wenzel, J. Hertkorn, M. Guo, T. Langen, and T. Pfau, Transient supersolid properties in an array of dipolar quantum droplets, *Phys. Rev. X* **9**, 011051 (2019).
- [57] Y. V. Kartashov, B. A. Malomed, and L. Torner, Metastability of quantum droplet clusters, *Phys. Rev. Lett.* **122**, 193902 (2019).
- [58] X. Zhang, X. Xu, Y. Zheng, Z. Chen, B. Liu, C. Huang, B. A. Malomed, and Y. Li, Semidiscrete quantum droplets and vortices, *Phys. Rev. Lett.* **123**, 133901 (2019).
- [59] B. Liu, H. Zhang, R. Zhong, X. Zhang, X. Qin, C. Huang, Y. Li, and B. A. Malomed, Symmetry breaking of quantum droplets in a dual-core trap, *Phys. Rev. A* **99**, 053602 (2019).
- [60] O. Morsch and M. Oberthaler, Dynamics of Bose-Einstein condensates in optical lattices, *Rev. Mod. Phys.* **78**, 179 (2006).
- [61] Y. Liu and S. Yang, Three-dimensional solitons in two-component Bose-Einstein condensates, *Chin. Phys. B* **23**, 110308 (2014).
- [62] R. Yang and J. Yang, Effect of interaction strength on gap solitons of Bose-Einstein condensates in optical lattices, *Chin. Phys. B* **17**, 1189 (2008).
- [63] Q. Wang, H. Yang, N. Su and L. Wen, Ground-state phases and spin textures of spin-orbit-coupled dipolar Bose-Einstein condensates in a rotating toroidal trap, *Chin. Phys. B* **29**, 116701 (2020).
- [64] Q. Cao and C. Dai, Symmetric and anti-symmetric solitons of the fractional second-and third-order nonlinear Schrödinger equation, *Chin. Phys. Lett.* **38**, 090501 (2021).
- [65] B. Li, Y. Zhao, S. Xu, Q. Zhou, Q. Fu, F. Ye, C. Hua, M. Chen, H. Hu, Q. Zhou and Z. Qiu, Two-dimensional gap solitons in parity-time symmetry Moiré optical lattices with Rydberg-Rydberg interaction, *Chin. Phys. Lett.* **40**, 044201 (2023).
- [66] R. Zhang, X. Zhang and L. Li, Exotic vortex structures of the dipolar Bose-Einstein condensates trapped in harmonic-like and toroidal potential, *Phys. Lett. A* **383**, 231 (2019).
- [67] J. Wang, W. Wang, X. Bai and S. Yang, Ring phases of spin-orbit coupled Bose-Einstein condensate in the radial optical lattices, *Eur. Phys. J. Plus* **134**, 27 (2019).
- [68] X. Zhang, M. Kato, W. Han, S. Zhang and H. Saito, Spin-orbit-coupled Bose-Einstein condensates held under a toroidal trap, *Phys. Rev. A* **95**, 033620 (2017).
- [69] M. Brtko, A. Gammal and B. A. Malomed, Hidden vorticity in binary Bose-Einstein condensates, *Phys. Rev. A* **82**, 053610 (2010).
- [70] L. Wen, H. Xiong and B. Wu, Hidden vortices in a Bose-Einstein condensate in a rotating double-well potential, *Phys. Rev. A* **82**, 053627 (2010).
- [71] S. Subramaniyan, Vortex formation and hidden vortices in dipolar Bose-Einstein condensates, *Phys. Lett. A* **381**, 3062 (2017).
- [72] C. Huang, L. Lyu, H. Huang, Z. Chen, S. Fu, H. Tan, B. A. Malomed and Y. Li, Dipolar bright solitons and solitary vortices in a radial lattice, *Phys. Rev. A* **96**, 053617 (2017).
- [73] Y. Zheng, S. Chen, Z. Huang, S. Dai, B. Liu, Y. Li and

- S. Wang, Quantum droplets in two-dimensional optical lattices, *Front. Phys.* **16**, 22501 (2021).
- [74] B. Liu, Y. Chen, A. Yang, X. Cai, Y. Liu, Z. Luo, X. Qin, X. Jiang, Y. Li and B. A. Malomed, Vortex-ring quantum droplets in a radially-periodic potential, *New J. Phys.* **24**, 123026 (2022).
- [75] B. Liu, X. Cai, X. Qin, X. Jiang, J. Xie, B. A. Malomed, and Y. Li, Ring-shaped quantum droplets with hidden vorticity in a radially periodic potential, *Phys. Rev. E* **108**, 044210 (2023).
- [76] J. Qin, G. Dong, and B. A. Malomed, Stable giant vortex annuli in microwave-coupled atomic condensates, *Phys. Rev. A* **94**, 053611 (2016).
- [77] A. Boudjemâa, Two-dimensional quantum droplets in dipolar Bose gases, *New J. Phys.* **21**, 093027 (2019).
- [78] F. Wächtler and L. Santos, Ground-state properties and elementary excitations of quantum droplets in dipolar Bose-Einstein condensates, *Phys. Rev. A* **94**, 043618 (2016).
- [79] A. Cidrim, F. E. A. dos Santos, E. A. L. Henn, and T. Macri, Vortices in self-bound dipolar droplets, *Phys. Rev. A* **98**, 023618 (2018).
- [80] A. Yang, G. Li, X. Jiang, Z. Fan, Z. Chen, B. Liu, and Y. Li, Two-dimensional quantum droplets in binary dipolar Bose-Bose mixture, *Photonics* **10**, 405 (2023).
- [81] G. Li, X. Jiang, B. Liu, Z. Chen, B. A. Malomed, and Y. Li, Two-dimensional anisotropic vortex quantum droplets in dipolar Bose-Einstein condensates, *Front. Phys.* **19**, 22202 (2024).
- [82] J. Huang, X. Jiang, H. Chen, Z. Fan, W. Pang and Y. Li, Quadrupolar matter-wave soliton in two-dimensional free space, *Front. Phys.* **10**, 1 (2015).
- [83] Y. Li, J. Liu, W. Pang, and B. A. Malomed, Lattice solitons with quadrupolar intersite interactions, *Phys. Rev. A* **88**, 063635 (2013).
- [84] R. Zhong, N. Huang, H. Li, H. He, J. Lü, C. Huang and Z. Chen, Matter-wave solitons supported by quadrupole-quadrupole interactions and anisotropic discrete lattices, *Int. J. Mod. Phys. B* **32**, 1850107 (2018).
- [85] J. M. Junquera-Hernández, J. Sánchez-Marín, and D. Maynau, Molecular electric quadrupole moments calculated with matrix dressed SDCl, *Chemical Physics Lett.* **359**, 343-348 (2002).
- [86] S. G. Bhongale, L. Mathey, E. Zhao, S. F. Yelin, and M. Lemeschko, Quantum phases of quadrupolar Fermi gases in optical lattices, *Phys. Rev. Lett.* **110**, 155301 (2013).
- [87] G. Chen, Y. Liu, H. Wang, Mixed-mode solitons in quadrupolar BECs with spin-orbit coupling, *Commun. Nonlinear Sci. Numer. Simulat* **48**, 318 (2017).
- [88] L. P. Pitaevskii L. P. and S. Stringari, *Bose-Einstein Condensation* (Oxford University Press, Oxford, 2003).
- [89] A Wang, S. Yi, Trapped Bose-Einstein condensates with quadrupole-quadrupole interactions, *Chin. Phys. B* **27**, 120307 (2018).
- [90] J. C. Smith, D. Baillie, P. B. Blakie, Quantum droplet states of a binary magnetic gas, *Phys. Rev. Lett.* **126**, 025302 (2021).
- [91] R. N. Bisset, L. A. Peña Ardila, and L. Santos, Quantum droplets of dipolar mixtures, *Phys. Rev. Lett.* **126**, 025301 (2021).
- [92] M. L. Chiofalo, S. Succi and M. P. Tosi, Ground state of trapped interacting Bose-Einstein condensates by an explicit imaginary-time algorithm, *Phys. Rev. E* **62**, 7438 (2000).
- [93] W. Z. Bao and Q. Du, Computing the ground state solution of Bose-Einstein condensates by a normalized gradient flow, *SIAM J. Sci. Comp.* **25**, 1674-1697 (2004).
- [94] J. K. Yang and T. I. Lakoba, Accelerated imaginary-time evolution methods for the computation of solitary waves, *Stud. Appl. Math.* **120**, 265 (2008).
- [95] N. G. Vakhitov and A. A. Kolokolov, Stationary solutions of the wave equation in media with nonlinearity saturation, *Radiophys Quantum Electron.* **16**, 783 (1973).
- [96] G. E. Astrakharchik and B. A. Malomed, Dynamics of one-dimensional quantum droplets, *Phys. Rev. A* **98**, 013631 (2018).
- [97] J. Hu, S. Li, Z. Chen, J. Lü, B. Liu, Y. Li, Discrete solitons in zigzag waveguide arrays with different types of linear mixing between nearest-neighbor and next-nearest-neighbor couplings, *Phys. Lett. A* **384**, 126448 (2020).
- [98] Z. Lin, X. Xu, Z. Chen, Z. Yan, Z. Mai, and B. Liu, Two-dimensional vortex quantum droplets get thick, *Commun. Nonlinear Sci. Numer. Simulat.* **93**, 105536 (2021).